α decay and cluster radioactivity in extreme laser fields

Hui Wang, Yingge Huang, Zepeng Gao, Jiali Huang, Erxi Xiao, Long Zhu, and Jun Su*
Sino-French Institute of Nuclear Engineering and Technology, Sun Yat-sen University, Zhuhai 519082, China
(Dated: December 8, 2024)

The potential of high-intensity lasers to influence nuclear decay processes has become a subject of considerable interest. This study quantitatively evaluates the effects of high-intensity lasers on α decay and cluster radioactivity. Our calculations reveal that among the parent nuclei investigated, ^{144}Nd is the most susceptible to laser-induced alterations, primarily due to its relatively low decay energy. Additionally, circularly polarized lasers exhibit a greater impact on decay modifications compared to linearly polarized lasers. Given the limited time resolution of current detectors, it is essential to account for the time-averaging effect of laser influences. Incorporating the effects of circular polarization, time-averaging, and angular-averaging, our theoretical predictions indicate that the modification of ^{144}Nd decay could reach 0.1% at an intensity of 10^{27} W/cm^2. However, this intensity far exceeds the current laser capability of 10^{23} W/cm^2, and the predicted modification of 0.1% remains below the detection threshold of contemporary measurement techniques. Observing laser-assisted α decay and ^{14}C cluster radioactivity will likely remain unfeasible until both ultrahigh laser intensities and significant advancements in experimental resolution are achieved.

Keywords: extreme laser field, the Frozen Hartree-Fock method, α decay, cluster radioactivity

I. INTRODUCTION

The field of research concerning the interactions of strong laser fields with atoms and molecules has reached a considerable degree of maturity [1–3]. Recently, projects for extremely high-intensity lasers have been proposed by the Shanghai Ultra Intensive Ultrafast Laser Facility [4, 5], the Extreme Light Infrastructure for Nuclear Physics [6, 7] and Russian group [8]. The further enhancements envisaged for the near future raise the interest in laser-driven nuclear physics, where extensive work has been done, such as the impact of laser fields on α decay [9–19], proton emission [6, 12, 20], cluster radioactivity [12, 18], nuclear fission [12], nuclear fusion [21–23] and nuclear excitation [24–26]. Among them, large attention has been paid to the α decay of the nuclei upon the influence of strong laser fields.

α decay is crucial in nuclear physics because it is capable of providing information on nuclear structure [27–29], and understanding popular topics such as the nuclear transformation between the liquid state and cluster state [30, 31]. α radioactivity was first discovered by Rutherford in 1903. Following this discovery, many attempts were made to modify α decay rates by changing temperature, pressure, magnetic and gravitational field [32, 33]. It turns out that the changes in the decay constant are quite small and can be neglected. The interpretations could stem from the Gamow picture of quantum mechanical tunneling [34]. Within this picture, α decay is correlated with the width through the potential. The distortions on potential and changes in decay energy modified by the above experiments are negligible, and no effect was detected. As the violent development is shown in laser technology, it provides an alternative method to explore and further this study.

Lasers interact with matter through two fundamental mechanisms: single photon interactions and electromagnetic field interactions. The former is not feasible for affecting nuclear processes because of the significant energy discrepancy between one single photon (on the order of 1 eV) and nuclear energy levels (on the order of 1 MeV). When the laser intensity is sufficiently high, the laser-matter interaction is predominantly governed by the electromagnetic field [3]. It is believed to possess the potential to control nuclear systems. Many works thus focused on how high-intensity laser is necessary to modify the decay processes [9–19]. According to Ref. [11], no significant modification of α decay is expected with the laser currently available or even in the forthcoming years.

However, some recent studies indicate a substantial effect of current laser intensities on α decay by solving the time-dependent Schrödinger equation within the oscillating Kramers-Henneberger frame [15–19]. Others suggest a small yet detectable influence at the current laser intensities or the intensity attained in the foreseeable future [9, 10, 12–14]. The inconsistencies in these findings highlight the ongoing debate and the lack of a clear consensus. Moreover, the temporal and angular effects and the variation of spatial shape of the laser field are intriguing for experiments, yet these remain ambiguous. In this work, we investigate the influence of extreme laser fields on nuclear α decay using the Frozen Hartree-Fock (FHF) approach [35–37]. In contrast to the aforementioned approaches, it can compute the microscopic internuclear potential and the deformation effects in a self-consistent way [38–40]. Cluster radioactivity has been investigated since 1984 [41] as an intermediate process between α decay and spontaneous fission [42–44], which deepens our understanding of decay mechanics. Thus, it is also interesting to study cluster radioactivity in this work.

This paper is organized as follows: Section II introduces the theoretical framework for laser-assisted

* sujun3@mail.sysu.edu.cn

particle decay using the Frozen Hartree-Fock method. Section III presents the results and discussions. Section IV gives the conclusions.

II. THEORETICAL FRAMEWORK

A. The unified formula of half-lives for α decay and cluster radioactivity

α decay and cluster radioactivity processes can be interpreted within a unified tunneling framework following Gamow's depiction [44–46]. The emitted particle is assumed to preform on the surface of the parent nucleus with varying preformation probability [47, 48] and eventually penetrate the potential barrier by constantly hitting it. The unified formula of half-lives for α decay and cluster radioactivity is expressed as

$$T_{1/2} = \frac{\hbar \ln 2}{FPS_{\rm pre}}, \tag{1}$$

where $\hbar$ is the reduced Planck constant, F represents the impinging frequency that hits the barrier, P denotes the penetration possibility and $S_{\rm pre}$ represents the preformation factor.

The impinging frequency F is expressed as

$$F = \frac{\sqrt{2E_k/\mu}}{R_{\rm in}}, \tag{2}$$

where $R_{\rm in}$ is the tunneling entrance point, and E_k is the kinetic energy of the emitted particle, which can be given by $E_k = \frac{A_d}{A_e+A_d}Q_e$. The reduced mass of the emitted particle and daughter nucleus μ is written as

$$\mu = \frac{A_e A_d}{A_e + A_d}, \tag{3}$$

where A_e and A_d are the masses of the emitted particle and daughter nucleus, respectively.

The penetration possibility P is determined using the Wentzel-Kramers-Brillouin (WKB) approximation. Taking into account the nuclear deformation effect, the total penetration possibility $P(t,\theta,I)$ is obtained by integrating $P(t,\phi,\theta,I)$ in all directions,

$$\begin{aligned} P(t,\theta,I) &= \frac{1}{2}\int_0^{\pi} P(t,\phi,\theta,I)\sin\phi d\phi, \\ P(t,\phi,\theta,I) &= \exp[-\frac{2(2\mu)^{1/2}}{\hbar}\int_{R_{\rm in}}^{R_{\rm out}} k(r,t,\phi,\theta,I)dr], \\ k(r,t,\phi,\theta,I) &= \sqrt{|V(r,t,\phi,\theta,I) - Q_e|}, \end{aligned} \tag{4}$$

where ϕ denotes the angle between the principal axis of the daughter nucleus and particle emission direction. θ represents the angle between the directions of the laser field and particle emission. I denotes the laser intensity. $R_{\rm in}$ and $R_{\rm out}$ are the tunneling entrance and exit points, respectively. These points are determined by the condition $V(r,t,\phi,\theta,I) = Q_e$, where Q_e is the decay energy of the emitted particle. $V(r,t,\phi,\theta,I)$ is the total potential with the intervention of laser field, which is expressed as

$$V(r,t,\phi,\theta) = V_N(r,\phi) + V_c(r,\phi) + V_l(r) + V_i(r,t,\phi,\theta,I), \tag{5}$$

where V_N and V_c are the nuclear potential and Coulomb potential, respectively. Both will be calculated by the Frozen Hartree-Fock method. The centrifugal potential V_l is given by

$$V_l(r) = \frac{l(l+1)\hbar^2}{2\mu r^2}, \tag{6}$$

where l is the corresponding angular momentum quantum number of emitted particle. The decay channel, decay energy, angular momentum, and experimental half-life are listed in Table I for clarity. V_i represents the interaction of the laser field with the decay system, which will be described in detail in the next subsection.

Uniform values or formulas of the preformation factor $S_{\rm pre}$ in Eq. (1) have been established [49–52]. For α decay, we adopt the following values [51]:

$$\begin{aligned} S_{\rm pre} &= 0.38 \text{ (even-even nuclei)}, \\ S_{\rm pre} &= 0.24 \text{ (odd-even nuclei)}, \\ S_{\rm pre} &= 0.13 \text{ (odd-odd nuclei)}. \end{aligned} \tag{7}$$

For cluster radioactivity [53], it is adopted as

$$\begin{aligned} S_{\rm pre} &= 10^{-0.01674 Z_e Z_d + 2.035466} \text{(even-even nuclei)}, \\ S_{\rm pre} &= 10^{-0.01674 Z_e Z_d + 2.035466 - 1.175} \text{(odd-A nuclei)}, \end{aligned} \tag{8}$$

where Z_e and Z_d are the proton number of the emitted particle and daughter nucleus, respectively.

B. The Frozen Hartree-Fock method

The nucleus-nucleus interaction potential, which consists of the nuclear potential V_N and the Coulomb potential V_c, is utilized to substitute the corresponding terms within Eq. (5). This potential is calculated using the Frozen Hartree-Fock (FHF) method, which requires frozen ground-state densities ρ_i of two nuclei at all distances. The resulting nucleus-nucleus interaction potential, referred to as the FHF potential in this context, is expressed as

$$V_{\rm FHF}(\boldsymbol{R}) = \int H[\rho_1(\boldsymbol{r}) + \rho_2(\boldsymbol{r}-\boldsymbol{R})]d\boldsymbol{r} - E[\rho_1] - E[\rho_2]. \tag{9}$$

The first term in the r.h.s. of Eq. (9) represents the total energy of the system when a distance vector $\boldsymbol{R}$ is placed between the centers of mass of two nuclei. $E[\rho_i]$ is the binding energy for each nucleus ($i = 1, 2$). To compute

the FHF potential, one has to first determine the Hartree-Fock ground states of two nuclei separately. The energy $E[\rho_i]$ is inherently obtained in the static Hartree-Fock process. Subsequently, the first term in the r.h.s. of Eq. (9) is calculated by placing the aforementioned two static Hartree-Fock solutions at a distance $\boldsymbol{R}$ from each other in a TDHF code [54–56] without a boost and computing the energy of the combined system, including the Coulomb contribution [57]. The above calculations are performed in a three-dimensional Cartesian geometry without symmetry assumptions and utilizing the Skyrme energy density functional Sly5 [58]. The box sizes for the Hartree-Fock calculations are selected to be 28^3 fm^3 and $28 \times 28 \times 100$ fm^3, respectively. The mesh spacing is 1.0 fm in all directions.

C. Laser-nucleus interaction

The laser field, known as the electromagnetic field, is treated as an electric field in this context. In fact, the magnetic part can be neglected since the sub-barrier motion of emitted particles under investigation remains nonrelativistic. Generally, the wavelength of the laser fields (near-ultraviolet to near-infrared) is much larger than the nuclear length scale (on the order of femtometre). The dipole approximation is thus allowed to be used for laser electric field, which is given in the length gauge as

$$V_i(r,t,\phi,\theta,I) = -Q_{\text{eff}}\boldsymbol{r}\boldsymbol{E}(t), \tag{10}$$

where

$$Q_{\text{eff}} = \frac{Z_e A_d - Z_d A_e}{A_e + A_d}, \tag{11}$$

is the effective charge, representing the tendency of the laser electric field to separate two nuclei in the decay system. Z_e and Z_d are the proton numbers of the emitted particle and daughter nucleus, respectively. The laser electric field also has an influence on the decay energy. Similarly, the change in decay energy ΔQ_e is expressed as

$$\Delta Q_e = eZ_e\boldsymbol{R}_d(\phi)\boldsymbol{E}(t), \tag{12}$$

where $\boldsymbol{R}_d$ is the radius of the daughter nucleus, along which the emitted particle penetrates. The decay energy induced by the laser field is thus given by

$$Q_e^* = Q_e + \Delta Q_e. \tag{13}$$

Besides, the time for emitted particles to penetrate through the potential barrier can be estimated. Considering α particle traveling through a barrier of width $l \simeq 50$ fm with decay energy 10 MeV, its traversal time is calculated to be around 10^{-21} s. While one optical cycle for the 800-nm laser field is on the order of femtoseconds. Consequently, the laser electric field can be treated in the quasistatic approximation, i.e., the laser field is viewed as static during particle penetration through the barrier.

The impact of the spatial shape of the laser on decay processes should be of interest. In this work, we consider two types of shapes of laser, which are expressed as follows

$$\begin{aligned}
&\boldsymbol{E}(t) = E_0\sin(\frac{2\pi ct}{\lambda})\boldsymbol{e}_r(\text{linear polarization}),\\
&\boldsymbol{E}(t) = E_0(\sin(\frac{2\pi ct}{\lambda})\boldsymbol{e}_x + \cos(\frac{2\pi ct}{\lambda})\boldsymbol{e}_y)(\text{circular polarization}),
\end{aligned} \tag{14}$$

where c is the speed of light and λ is the laser wavelength (800 nm is used here). The peak electric field strength E_0 can be represented by the laser intensity I, which is given by

$$E_0[\text{V/cm}] = 27.44(I[\text{W/cm}^2])^{1/2}. \tag{15}$$

D. The relative change of penetration possibility ΔP

The Frozen Hartree-Fock method ignores the dynamical effects and the Pauli repulsion between the nucleons belonging to the different nuclei [40, 57]. The latter is regarded as a significant factor in the preformation of emitted particles on the surface of the parent nucleus. Moreover, our model is incapable of calculating the preformation factor, which remains a great challenge for beyond-mean field theory as well. Therefore, this work focuses on the relative change of penetration possibility induced by the laser field, while ignoring the impact of the laser field on the preformation factor [11–14]. The relative change of penetration possibility is defined as

$$\Delta P(t,\theta,I) = \frac{P(t,\theta,I) - P(t,\theta,I=0)}{P(t,\theta,I=0)}. \tag{16}$$

It should be noted that ΔP is a function of time t, emission angle θ and intensity I. It is intriguing to consider the temporal and angular effects of the laser field. The time-integrated modification of penetration possibility is expressed as

$$\overline{\Delta P}_t(\theta,I) = \frac{1}{T}\int_0^T \Delta P(t,\theta,I)dt. \tag{17}$$

The time-integrated and angle-integrated modification is expressed as

$$\overline{\Delta P}_{t\theta}(I) = \frac{1}{2}\int_0^\pi d\theta\overline{\Delta P_t}(\theta,I)\sin\theta. \tag{18}$$

To shed light on the laser-modification of penetration possibility, it is necessary to further the formula of ΔP.

We start from the penetration possibility $P(t,\phi,\theta,I)$:

$$\begin{aligned} P(t,\phi,\theta,I) &= \exp\left[-\frac{2(2\mu)^{1/2}}{\hbar}\int_{R_{\rm in}}^{R_{\rm out}} \right. \\ &\left.\times\sqrt{V(r,t,\phi,\theta,I)-Q_e^*}dr\right] \\ &= \exp\left[-\frac{2(2\mu)^{1/2}}{\hbar}\int_{R_{\rm in}}^{R_{\rm out}}\sqrt{V_0(r)}\right. \\ &\left.\times\sqrt{1+\frac{V_i(r,t,\phi,\theta,I)-\Delta Q}{V_0(r)}}dr\right], \end{aligned} \tag{19}$$

with $V_0(r)=V_{\rm FHF}(r)+V_l(r)-Q_e$. Assuming that $|V_i-\Delta Q|\ll V_0$, we proceed with the Taylor expansion of Eq. (19)

$$\begin{aligned} P(t,\phi,\theta,I) &\approx \exp\left[\gamma^{(0)}+\gamma^{(1)}+\gamma^{(2)}\right] \\ &= \exp(\gamma^{(0)})\exp(\gamma^{(1)}+\gamma^{(2)}), \end{aligned} \tag{20}$$

where $\gamma^{(0)}$, $\gamma^{(1)}$ and $\gamma^{(2)}$ are given by

$$\begin{aligned} \gamma^{(0)} &= -\frac{2(2\mu)^{1/2}}{\hbar}\int_{R_{\rm in}}^{R_{\rm out}} dr\sqrt{V_0(r)}, \\ \gamma^{(1)} &= -\frac{(2\mu)^{1/2}}{\hbar}\int_{R_{\rm in}}^{R_{\rm out}} dr\frac{V_i(r,t,\phi,\theta,I)-\Delta Q}{\sqrt{V_0(r)}}, \\ \gamma^{(2)} &= \frac{(2\mu)^{1/2}}{\hbar}\int_{R_{\rm in}}^{R_{\rm out}} dr\frac{(V_i(r,t,\phi,\theta,I)-\Delta Q)^2}{4V_0^{3/2}(r)}. \end{aligned} \tag{21}$$

Note that $\exp(\gamma^{(0)})$ is approximately equal to the laser-free penetration possibility $P(t,\phi,\theta,I=0)$, the relative change of penetration possibility can be given by

$$\begin{aligned} \Delta P(t,\phi,\theta,I) &\approx \frac{\exp(\gamma^{(0)})\exp(\gamma^{(1)}+\gamma^{(2)})-\exp(\gamma^{(0)})}{\exp(\gamma^{(0)})} \\ &= \exp(\gamma^{(1)}+\gamma^{(2)})-1 \\ &\approx \gamma^{(1)}+\gamma^{(2)}. \end{aligned} \tag{22}$$

$\gamma^{(1)}+\gamma^{(2)}$ tends to zero as we have assumed that $|V_i-\Delta Q|\ll V_0$. Given the analysis of diverse spatial profiles of the laser in this work, it is necessary to provide detailed formulations for $\gamma^{(1)}$ and $\gamma^{(2)}$. For linear polarization, it reads

$$\begin{aligned} \gamma^{(1)} &= \frac{27.44(2\mu)^{1/2}}{\hbar}\sqrt{I}\sin(\frac{2\pi ct}{\lambda})\cos\theta \\ &\times\int_{R_{\rm in}}^{R_{\rm out}} dr\frac{Q_{\rm eff}r+eZ_eR_{\rm in}(\phi)}{\sqrt{V_0(r)}}, \\ \gamma^{(2)} &= \frac{188.24(2\mu)^{1/2}}{\hbar}I\sin^2(\frac{2\pi ct}{\lambda})\cos^2\theta \\ &\times\int_{R_{\rm in}}^{R_{\rm out}} dr\frac{(Q_{\rm eff}r+eZ_eR_{\rm in}(\phi))^2}{V_0^{3/2}(r)}. \end{aligned} \tag{23}$$

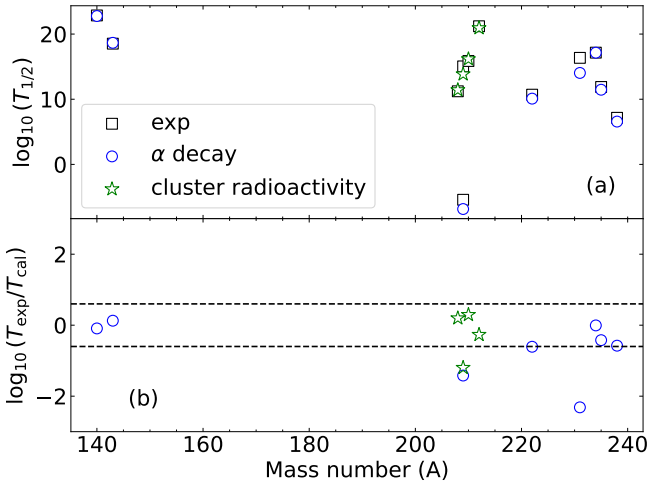

FIG. 1. (a) Experimental and calculated half-lives for different parent nuclei. The black squares represent the experimental data. The blue circles represent the calculated α decay half-lives of the ground state parent nuclei ^{144}Nd, ^{226}Ra, ^{238}U, ^{242}Cm, ^{147}Sm, ^{213}Po, ^{235}U, and ^{239}Pu. The green stars represent the calculated ^{14}C cluster radioactivity half-lives of the ground state parent nuclei ^{222,223,224,226}Ra. (b) The corresponding logarithms of hindrance factors (HF $=T_{\rm exp}/T_{\rm cal}$).

For circular polarization, it reads

$$\begin{aligned} \gamma^{(1)} &= \frac{27.44(2\mu)^{1/2}}{\hbar}\sqrt{I}(\sin(\frac{2\pi ct}{\lambda})\cos\theta+\cos(\frac{2\pi ct}{\lambda})\sin\theta) \\ &\times\int_{R_{\rm in}}^{R_{\rm out}} dr\frac{Q_{\rm eff}r+eZ_eR_{\rm in}(\phi)}{\sqrt{V_0(r)}}, \\ \gamma^{(2)} &= \frac{188.24(2\mu)^{1/2}}{\hbar}I(\sin(\frac{2\pi ct}{\lambda})\cos\theta+\cos(\frac{2\pi ct}{\lambda})\sin\theta)^2 \\ &\times\int_{R_{\rm in}}^{R_{\rm out}} dr\frac{(Q_{\rm eff}r+eZ_eR_{\rm in}(\phi))^2}{V_0^{3/2}(r)}. \end{aligned} \tag{24}$$

III. RESULTS

Figure 1 (a) shows the comparison between the experimental and theoretical half-lives. The corresponding deviations between the logarithms of the experimental half-lives and the calculated values are depicted in Fig. 1 (b). The blue circles represent the calculated α decay of the ground state parent nuclei ^{144}Nd, ^{226}Ra, ^{238}U, ^{242}Cm, ^{147}Sm, ^{213}Po, ^{235}U, and ^{239}Pu. The green stars represent the calculated ^{14}C cluster radioactivity of the ground state parent nuclei ^{222,223,224,226}Ra. It can be seen that the difference between the calculated values and experimental data is small. The values of $\log_{10}(T_{\rm exp}/T_{\rm cal})$ for α decay and cluster radioactivity are generally within the range of about ±0.6. These correspond to the values of the ratio $T_{\rm exp}/T_{\rm cal}$ within the range of about 0.25-3.98. It demonstrates the reliability of our model to predict

TABLE I. Experimental and calculated half-lives (in seconds) of α decay and cluster radioactivity. Q_e and l are the decay energy and the angular momentum quantum number of the emitted particle, respectively. The hindrance factor (HF) is defined as the ratio between the experimental and calculated half-lives (HF = $T_{\rm exp}/T_{\rm cal}$).

Decay channels	Q_e(MeV)	l	$\log_{10}T_{\rm exp}$	$\log_{10}T_{\rm cal}$	$\log_{10}$HF
^{144}Nd $\rightarrow$ ^{140}Ce+α	1.90	0	22.86	22.77	0.09
^{226}Ra $\rightarrow$ ^{222}Rn+α	4.87	0	10.70	10.09	0.61
^{238}U $\rightarrow$ ^{234}Th+α	4.27	0	17.15	17.14	0.01
^{242}Cm $\rightarrow$ ^{238}Pu+α	6.23	0	7.15	6.57	0.58
^{147}Sm $\rightarrow$ ^{143}Nd+α	2.31	0	18.53	18.66	-0.13
^{213}Po $\rightarrow$ ^{209}Pb+α	8.54	0	-5.43	-6.85	1.42
^{235}U $\rightarrow$ ^{231}Th+α	4.68	1	16.35	14.04	2.31
^{239}Pu $\rightarrow$ ^{235}U+α	5.25	3	11.88	11.46	0.42
^{222}Ra $\rightarrow$ ^{208}Pb+^{14}C	33.05	0	11.22	11.42	-0.20
^{223}Ra $\rightarrow$ ^{209}Pb+^{14}C	31.83	4	15.04	13.84	1.20
^{224}Ra $\rightarrow$ ^{210}Pb+^{14}C	30.53	0	15.87	16.16	0.29
^{226}Ra $\rightarrow$ ^{212}Pb+^{14}C	28.20	0	21.20	20.93	0.27

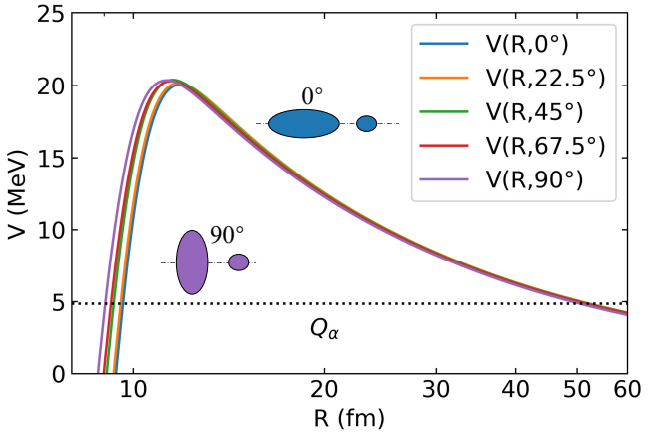

FIG. 2. Frozen Hartree-Fock potential for the α+^{222}Rn system with different orientations of ^{222}Rn. In particular, 0° and 90° represent tip and side orientation, respectively. Q_α is the experimental α-decay energy.

the half-lives. Detailed information on experimental and calculated data is listed in Table I.

One typically assumes a spherical shape for nuclei to simplify the calculation of α decay half-lives. However, it is reported that nuclear deformations can significantly influence these calculations [50, 51]. Figure 2 displays the FHF potential for α+^{222}Rn for selected orientations. Since α particle is spherical, the differences of these potentials stem from the orientations of daughter nucleus ^{222}Rn. It shows that as the orientation rotates from tip to side, the Coulomb barrier increases and the nuclear part of the potential becomes shallower. This phenomenon can be attributed to the larger overlap of nuclear density distribution at the tip orientation, which leads to a more pronounced effect of the nuclear potential. It also shows that the tunneling points differ by approximately

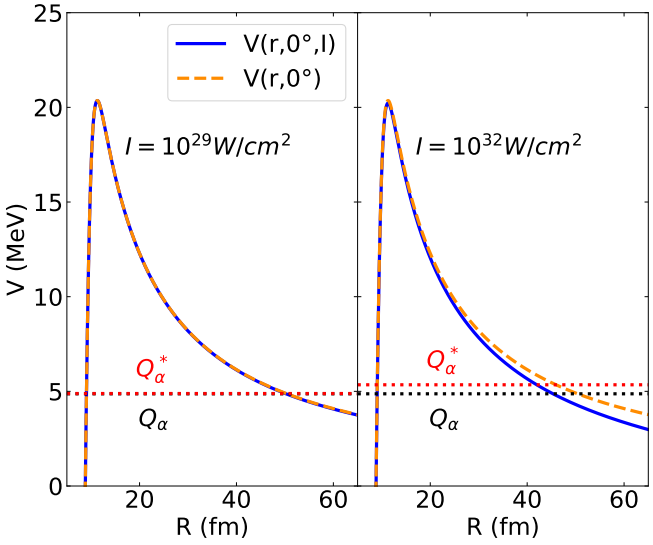

FIG. 3. The comparison between laser-free and laser-modified internuclear potentials for α+^{222}Rn system under two laser intensities, $I = 10^{29}$ W/cm^2 and 10^{32} W/cm^2. 0° represents the tip orientation of ^{222}Rn. The solid line stands for the laser-modified case, dashed line stands for the laser-free case. The dotted line represents the α emission energy, where Q_α is the experimental α decay energy, and Q_α^* is the energy of emitted α particle accelerated by the laser field.

1 fm with varying orientations, resulting in an order of magnitude change in the penetration probability and subsequent alterations in α decay half-lives. In addition, laser-nucleus interaction depends on the angle between the directions of the laser field and particle emission. It is inferred that nuclear deformation is a critical factor that should be incorporated in laser-assisted α decay as well as cluster radioactivity calculation.

To illustrate the influence of the laser field on the penetration process, the comparison of laser-free internuclear potentials for α+^{222}Rn system with two laser-assisted cases is shown in Fig. 3. For the sake of simplicity, only the tip orientation case is represented. The laser field induces a downward shift in the Coulomb part of the potential and an elevation in the α-decay energy, while its impact on the nuclear part remains negligible. This is not surprising because the intense laser field of intensity 10^{32} W/cm^2 (10^{29} W/cm^2) is comparable to the Coulomb field strength from the daughter nucleus ^{222}Rn at a distance of about 66 fm (371 fm). The Coulomb part is defeated by the nuclear part within the core. Therefore, the laser field alters the tunneling points by deforming the long-range Coulomb part of the potential and changing the energy of the emitted particle, which consequently affects the penetration probability.

It is also seen from Fig. 3 that the modification by the laser field becomes observable only when the intensity reaches 10^{32} W/cm^2. Given the current laser technology, no significant modifications of half-lives

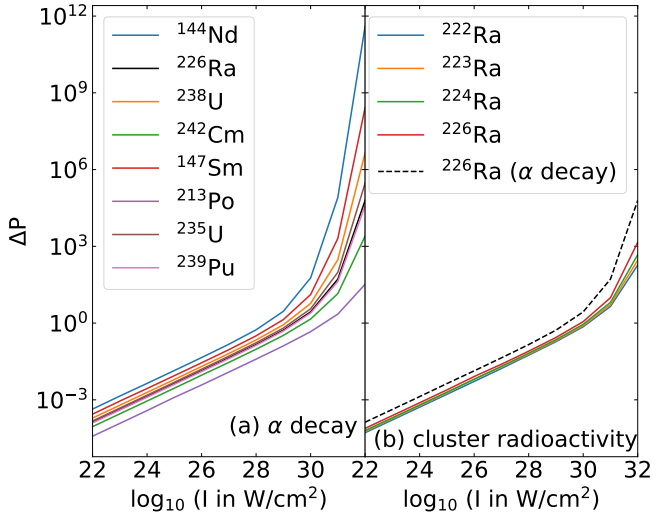

FIG. 4. Relative change of penetration possibility $\Delta P(t_0, \theta_0, I)$ for (a) α decay and (b) ^{14}C cluster radioactivity at the moment t_0 of the peak electric field strength with a fixed angle $\theta_0 = 0°$. Dashed line in (b) represents ΔP for α decay of parent nucleus ^{226}Ra.

would be observed experimentally. Nevertheless, even subtle alterations in the potential or decay energy may give rise to discernible effects on the decay processes, since the tunneling is highly sensitive to the internuclear potential. It is demonstrated in Fig. 4. The relative change of penetration probability ΔP could reach 10^{-3} within the laser intensity accessible. In Fig. 4, ΔP is obtained at the moment of the peak electric field strength with a fixed angle $\theta = 0°$. ΔP and laser intensity I are plotted in the logarithmic scale. As depicted in Fig. 4, the lower the decay energy a parent nucleus has, the greater the relative change in its penetration possibility across different nuclei. Obviously, the parent nucleus ^{144}Nd is quite susceptible to laser-induced modification. This stems from its relatively low α decay energy, which results in an extended tunneling path, allowing the laser field to exert a prolonged influence on the decay process. At the intensity of 10^{24} W/cm^2, the modification of penetration possibility is on the order of 0.1% for ^{144}Nd, which is in agreement with Ref. [10, 12].

The laser-assisted α decay modifications for even-even nuclei also show good agreement with the predictions in Ref. [13, 14]. The above calculations are conducted utilizing the same approximations (dipole and quasistatic approximation) for the laser field and various internuclear potentials. Some studies[10, 12–14] employ the phenomenological internuclear potentials, while this work utilizes the microscopic potential and takes into account the nuclear deformation effects. Although the results are similar, the FHF method helps pursue a more microscopic understanding of laser-assisted α decay and cluster radioactivity in a self-consistent manner. Additionally, in contrast to the modest impact of the laser field predicted by our model, several studies [15–19] suggest a significant alteration of alpha decay processes under current laser intensities. These calculations are obtained by solving the time-dependent Schrödinger equation within the oscillating Kramers-Henneberger frame. The critical assumption in them is the continuity of the laser field, whereas this work is based on the premise of a single laser pulse. This main discrepancy in laser conditions results in substantial differences in the respective predictions. However, the high-intensity and continuous laser field is unattainable. The potential for future technological advancements in continuous laser technology presents an intriguing area for exploration, with the promise of inducing more pronounced modifications in α decay processes.

The comparison of ΔP between α decay and cluster radioactivity for the same parent nucleus ^{226}Ra is made. As shown in Fig. 4(b), ΔP for α decay is larger than that for cluster radioactivity of any parent nucleus shown here. This could be illustrated by the sensitivity of tunneling to the change of potential and decay energy. As is known, α (^{14}C cluster) decay energies used here are around 5 MeV (30 MeV), and the tunneling exit points for α (^{14}C cluster) are around 60 fm (25 fm). This means that the modifications of the laser field in potential and decay energy for α decay have a larger impact on decay processes, and subsequently higher relative change of penetration possibility. Besides, it also shows linear dependence of ΔP on laser intensity, while the values of slope change dramatically after 10^{30} W/cm^2. This can be explained by Eq. (22) and Eq. (23) or Eq. (24). For relatively low intensities, ΔP is proportional to $\sqrt{I}$. Only for intense intensities, the term $\gamma^{(2)}$ proportional to I is not negligible, leading to an inflection in the curves. It should be noted that the slope of ΔP versus the intensity curve is steeper for alpha decay at extreme intensities. This indicates a higher sensitivity of alpha decay to intense laser intensities. Given the heightened sensitivity, it is reasonable to extrapolate that the effect of laser acceleration on proton emission should be even more pronounced. Consequently, it is recommended to utilize laser-accelerated proton emission as a diagnostic tool to assess the impact of intense laser field.

The theoretical calculations above are implemented at the peak laser electric field strength and a fixed angle $\theta = 0°$. Figure 5 shows the linearly polarized laser electric field strength E and relative modification of penetration possibility ΔP at a fixed angle $\theta = 0°$ as a function of time. It is clear that time-dependent E_t and ΔP share a similar trend of variation, which can be explained by Eq. (22) and Eq. (23). Theoretically, the laser promotion and suppression effects on the penetration possibility can be observed throughout a laser pulse circle. However, the best time resolution of the experimental detector is on the order of nanoseconds, which is much larger than the current laser period (on the order of femtoseconds). This means we cannot observe the time-dependent alteration of ΔP shown in Fig. 5 (b), but a time averaging result in practice. Therefore, it is necessary to take into account

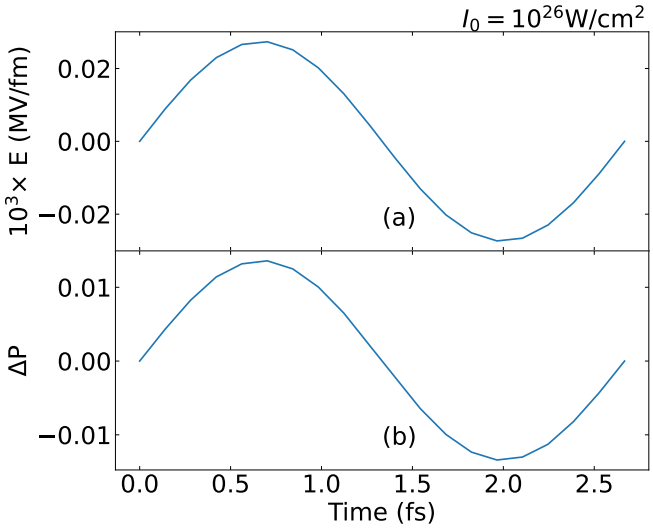

FIG. 5. (a) Linearly polarized laser electric field strength E and (b) relative modification of penetration possibility $\Delta P(t, \theta_0, I_0)$ at a fixed angle $\theta_0 = 0^\circ$ as a function of time. The intensity I_0 is 10^{26} W/cm^2 here for α+^{222}Rn system.

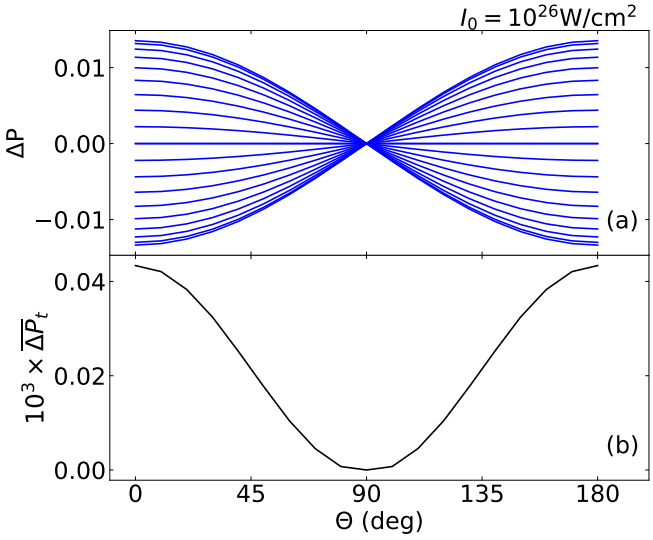

FIG. 6. (a) Relative changes of penetration possibility $\Delta P(t, \theta, I_0)$ as a function of angle θ seen from one pulse circle. Various curves depict the scenario at a specific moment t within the pulse cycle. (b) Time-integrated modification $\overline{\Delta P}_t(\theta, I_0)$ as a function of angle θ. θ represents the angle between the directions of the laser field and particle emission. Linear polarization is used here for system α+^{222}Rn at the intensity of $I_0 = 10^{26}$W/cm^2.

the effect of a complete laser period on ΔP.

Figure 6(a) displays the correlation between ΔP and θ for a pulse circle. As illustrated in Eq. (23), ΔP exhibits a linear correlation with cosθ at some moment t. It explains large variations of ΔP around 0° and 180°, and no modification along 90°. Along one fixed angle, ΔP looks quite symmetric to be canceled by integrating

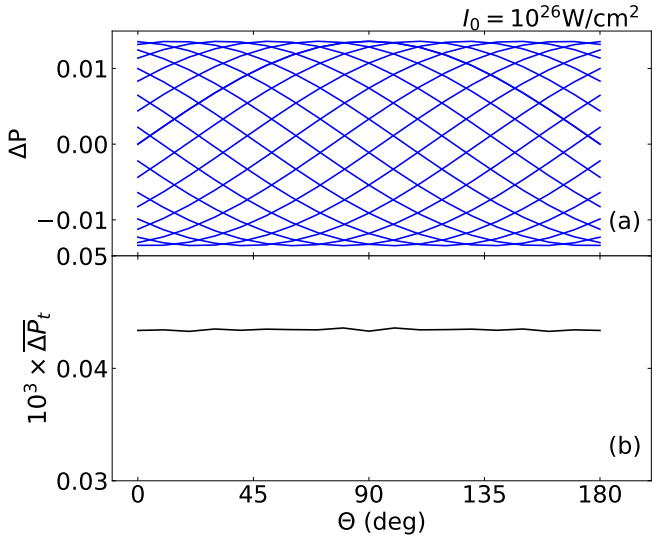

FIG. 7. The same as Fig. 6 but for circular polarization.

time. Then no net gain would be left for modification. Figure 6(b) shows time-integrated modification $\overline{\Delta P}_t$ as a function of angle θ. We can infer that some small asymmetries do exist so that a residual net gain remains. This can be seen from Eq. (23) that the first equation, involving $\sin(\frac{2\pi c}{\lambda}t)$, cancels out over time, whereas the second equation keeps positive throughout the laser period, contributing to the net gain. The time-integrated modifications are strongest along 0° and 180°, which are three orders of magnitude smaller than that before integration though.

Some studies [59, 60] have explored the potential of elliptically polarized lasers in harnessing more information from the realm of strong-field atomic physics. The circular polarization, a specific manifestation of elliptical polarization, is taken into account. Figure 7(a) shows the correlation between ΔP and θ for a pulse circle with circular polarization. Unlike the linear polarized case, ΔP in circular polarization arises from the superposition of sinθ and cosθ, leading to uniformly distributed modifications across all angles. The time-integrated result is represented in Fig. 7(b). It can be seen that time-integrated modification $\overline{\Delta P}_t$ is not affected by the angle between the directions of the laser field and particle emission, emphasizing the advantage of the circular polarization to render the modification of penetration possibility free from time averaging. This view coincides with that proposed by Qi *et al.* [10] who recommend the elliptically polarized laser comparing to the linear polarized case.

As was shown in Fig. 6, the linearly polarized laser results in angular anisotropy, with the most significant modifications along 0° and 180°. The comparison of the time-integrated modification $\overline{\Delta P}_t$ along 0° between linear and circular polarizations is displayed in Fig. 8(a). It is observed that both exhibit consistent behavior. In other words, the time-integrated modification $\overline{\Delta P}_t$

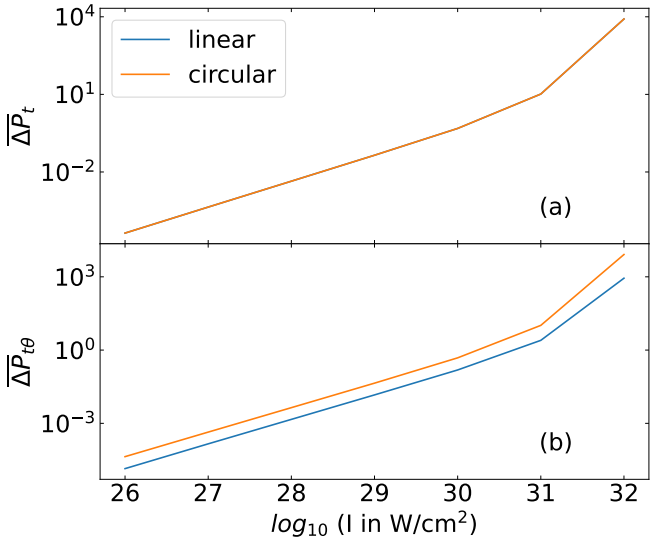

FIG. 8. (a) Time-integrated modification $\overline{\Delta P}_t(\theta = 0°, I)$ and (b) time-integrated and angle-integrated modification $\overline{\Delta P}_{t\theta}(I)$ using two polarization methods. The system is α+^{222}Rn.

TABLE II. The laser intensity I for α decay and cluster radioactivity when the time-integrated and angle-integrated modification $\overline{\Delta P}_{t\theta}$ reaches the order of magnitude of 10^{-3}. Circular polarization is employed here.

Decay channel	$\log_{10}I$	$\overline{\Delta P}_{t\theta}$
^{144}Nd $\rightarrow$ ^{140}Ce+α	27	4.66×10^{-3}
^{226}Ra $\rightarrow$ ^{222}Rn+α	28	4.39×10^{-3}
^{238}U $\rightarrow$ ^{234}Th+α	28	9.51×10^{-3}
^{242}Cm $\rightarrow$ ^{238}Pu+α	28	1.97×10^{-3}
^{147}Sm $\rightarrow$ ^{143}Nd+α	27	1.84×10^{-3}
^{213}Po $\rightarrow$ ^{209}Pb+α	29	3.48×10^{-3}
^{235}U $\rightarrow$ ^{231}Th+α	28	5.92×10^{-3}
^{239}Pu $\rightarrow$ ^{235}U+α	28	3.89×10^{-3}
^{222}Ra $\rightarrow$ ^{208}Pb+^{14}C	29	7.28×10^{-3}
^{223}Ra $\rightarrow$ ^{209}Pb+^{14}C	29	8.58×10^{-3}
^{224}Ra $\rightarrow$ ^{210}Pb+^{14}C	28	1.03×10^{-3}
^{226}Ra $\rightarrow$ ^{212}Pb+^{14}C	28	1.43×10^{-3}

in circular polarization maintains the maximum value observed in linear polarization throughout the entire range of angles. This indicates that the primary distinction in the modification induced by these two types of polarized lasers is predominantly associated with their angular distribution characteristics. Xiao et al. [14] point out that it is important to consider angular integration since nuclei often appear as a population. The time-integrated and angle-integrated modification $\overline{\Delta P}_{t\theta}$ is represented in Fig. 8(b). Obviously, the modification of circular polarization is several times larger than that of the linear case at the same intensity. It is preferable to employ the circularly polarized laser for a more significant modification.

Figure 9 displays time-integrated modification $\overline{\Delta P}_t$ along 0° for (a)(c) α decay and (b)(d) ^{14}C cluster

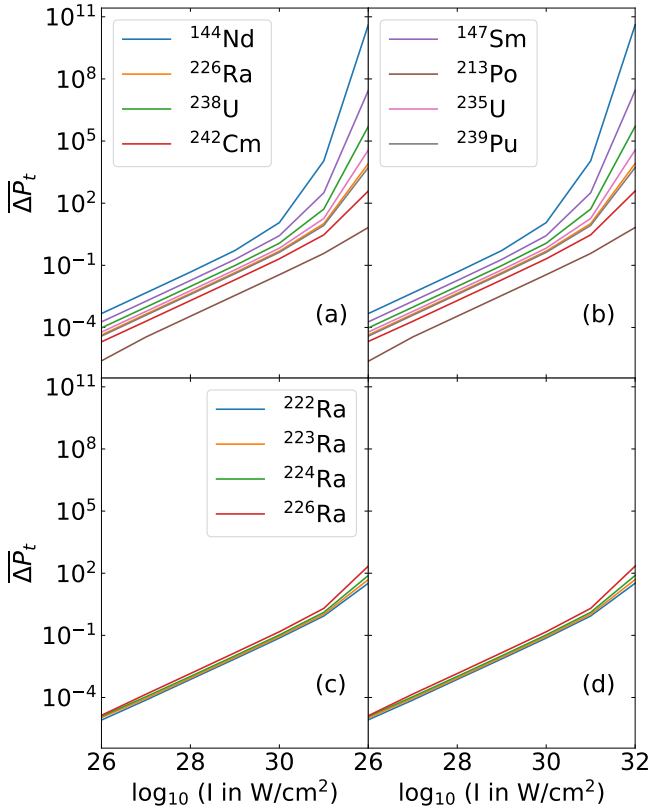

FIG. 9. Time-integrated modification $\overline{\Delta P}_t(\theta = 0°, I)$ for (a)(c) α decay and (b)(d) ^{14}C cluster radioactivity. The left and right panels refer to the linear and circular polarization, respectively.

radioactivity across different nuclei. The left and right panels refer to the linear and circular polarization, respectively. Similar to Fig. 8(a), the two polarizations show the same behavior when the angle θ is fixed at 0°. Among these nuclei, ^{144}Nd remains the most susceptible parent nucleus to laser-induced modification, which is attributed to its relatively low decay energy. Its modification attains a value of 0.1% at the intensity of 10^{27} W/cm^2, which significantly exceeds the current laser intensity of 10^{23} W/cm^2. While a higher intensity of 10^{28} W/cm^2 is required for ^{14}C cluster radioactivity. It should be noted that more physical effects are expected to be considered when the intensity approaches or surpasses the Schwinger critical field strength [61], whose corresponding laser intensity is 2.3×10^{29} W/cm^2. The laser intensity I for circular polarization where the time-integrated and angle-integrated modification $\overline{\Delta P}_{t\theta}$ reaches an order of magnitude of 10^{-3}, is detailed in Table II. It indeed exhibits consistent results with the scenario at $\theta = 0°$. The modifications reach the order of 0.1% at an intensity of 10^{27} W/cm^2 for α decay and 10^{28} W/cm^2 for cluster radioactivity. Consequently, it is evident that laser-assisted α decay and ^{14}C cluster radioactivity are not practically achievable with current technology.

IV. CONCLUSION

In this study, we conduct a comprehensive microscopic analysis of the effects of extreme laser fields on α decay and cluster radioactivity. Our primary objective is to quantitatively assess the influence of intense laser fields, accounting for their temporal and angular effects as well as variations in spatial structure. The theoretical framework is based on the Gamow model of quantum mechanical tunneling, while the Frozen Hartree-Fock method provides a self-consistent description of the internuclear potential and nuclear deformation effects. The laser-nucleus interaction is represented by an electric field under the dipole approximation.

Our findings indicate that the laser field induces a downward shift in the Coulomb component of the potential and an increase in decay energy. Given the high sensitivity of quantum tunneling to internuclear potential changes, even minor alterations in the potential or decay energy yield significant effects on the penetration probability. At an intensity of 10^{24} W/cm^2, the modification in penetration probability for the relevant nuclei reaches approximately 0.1%, aligning with results reported in Ref. [10].

The time- and angle-dependent modifications of penetration probability are analyzed under both linearly and circularly polarized lasers. In the case of linearly polarized lasers, the penetration probability exhibits its maximum modification at angles of 0° and 180°, with no modification at 90°. Conversely, circularly polarized lasers produce uniformly distributed modifications across all angles, with the angle-integrated modification induced by circular polarization being several times greater than that produced by linear polarization at the same intensity. Nevertheless, the time-integrated modifications decrease by three orders of magnitude after integration.

Finally, we compare the time- and angle-integrated modification of the penetration probability induced by circularly polarized lasers for both α decay and ^{14}C cluster radioactivity across various nuclei. Among the studied nuclei, ^{144}Nd is the most susceptible to laser-induced modifications, primarily due to its relatively low decay energy. At an intensity of 10^{27} W/cm^2, the modification in $\overline{\Delta P}_{t\theta}$ for ^{144}Nd reaches approximately 0.1%. However, this intensity far exceeds the current achievable laser intensity of 10^{23} W/cm^2, and a 0.1% modification remains below the detection threshold of current measurement precision. The effect in the ^{14}C cluster is more weak.

In conclusion, achieving observable laser-assisted α decay and ^{14}C cluster radioactivity will require future advancements in laser technology to significantly enhance intensity and experimental resolution. Consequently, expectations regarding the feasibility of laser-induced mechanisms for recycling nuclear radioactive waste should be carefully calibrated in light of these technological constraints.

ACKNOWLEDGMENTS

This work was supported by the National Natural Science Foundation of China under Grants Nos. 12475136 and 12075327.

[1] T. Brabec and H. Kapteyn, *Strong field laser physics*, Vol. 1 (Springer, 2008).
[2] M. A. Marques and E. K. Gross, Annu. Rev. Phys. Chem. **55**, 427 (2004).
[3] H. Schwoerer, J. Magill, and B. Beleites, *Lasers and nuclei: Applications of ultrahigh intensity lasers in nuclear science*, Vol. 694 (Springer Science & Business Media, 2006).
[4] W. Li, Z. Gan, L. Yu, C. Wang, Y. Liu, Z. Guo, L. Xu, M. Xu, Y. Hang, Y. Xu, *et al.*, Optics letters **43**, 5681 (2018).
[5] L. Yu, Y. Xu, Y. Liu, Y. Li, S. Li, Z. Liu, W. Li, F. Wu, X. Yang, Y. Yang, *et al.*, Optics express **26**, 2625 (2018).
[6] Ş. Mişicu and M. Rizea, Journal of Physics G: Nuclear and Particle Physics **46**, 115106 (2019).
[7] K. Tanaka, K. Spohr, D. Balabanski, S. Balascuta, L. Capponi, M. Cernaianu, M. Cuciuc, A. Cucoanes, I. Dancus, A. Dhal, *et al.*, Matter and Radiation at Extremes **5** (2020).
[8] A. Bashinov, A. Gonoskov, A. Kim, G. Mourou, and A. Sergeev, The European Physical Journal Special Topics **223**, 1105 (2014).
[9] H. M. C. Cortés, C. Müller, C. H. Keitel, and A. Pálffy, Physics Letters B **723**, 401 (2013).
[10] J. Qi, T. Li, R. Xu, L. Fu, and X. Wang, Physical Review C **99**, 044610 (2019).
[11] A. Pálffy and S. V. Popruzhenko, Physical Review Letters **124**, 212505 (2020).
[12] J. Qi, L. Fu, and X. Wang, Physical Review C **102**, 064629 (2020).
[13] J.-H. Cheng, W.-Y. Zhang, Q. Xiao, J.-G. Deng, and T.-P. Yu, Physics Letters B **848**, 138322 (2024).
[14] Q. Xiao, J.-H. Cheng, Y.-Y. Xu, Y.-T. Zou, J.-G. Deng, and T.-P. Yu, Nuclear Science and Techniques **35**, 27 (2024).
[15] Ş. Mişicu and M. Rizea, Journal of Physics G: Nuclear and Particle Physics **40**, 095101 (2013).
[16] D. Delion and S. Ghinescu, Physical Review Letters **119**, 202501 (2017).
[17] D. P. Kis and R. Szilvasi, Journal of Physics G: Nuclear and Particle Physics **45**, 045103 (2018).
[18] D. Bai, D. Deng, and Z. Ren, Nuclear Physics A **976**, 23 (2018).
[19] S. Ghinescu and D. Delion, Physical Review C **101**, 044304 (2020).
[20] J.-H. Cheng, Y. Li, and T.-P. Yu, Physical Review C **105**, 024312 (2022).

[21] F. Queisser and R. Schützhold, Physical Review C **100**, 041601 (2019).
[22] W. Lv, H. Duan, and J. Liu, Physical Review C **100**, 064610 (2019).
[23] S. Liu, H. Duan, D. Ye, and J. Liu, Physical Review C **104**, 044614 (2021).
[24] A. Pálffy and H. A. Weidenmüller, Physical Review Letters **112**, 192502 (2014).
[25] L. von der Wense, B. Seiferle, S. Stellmer, J. Weitenberg, G. Kazakov, A. Pálffy, and P. G. Thirolf, Physical Review Letters **119**, 132503 (2017).
[26] W. Wang, J. Zhou, B. Liu, and X. Wang, Physical Review Letters **127**, 052501 (2021).
[27] A. N. Andreyev, M. Huyse, P. Van Duppen, C. Qi, and et al., Physical Review Letters **110**, 242502 (2013).
[28] Y. T. Oganessian, F. S. Abdullin, P. D. Bailey, D. E. Benker, M. E. Bennett, S. N. Dmitriev, *et al.*, Physical Review Letters **104**, 142502 (2010).
[29] A. Sobiczewski and K. Pomorski, Progress in Particle and Nuclear Physics **58**, 292 (2007).
[30] T. Otsuka, T. Abe, T. Yoshida, Y. Tsunoda, N. Shimizu, N. Itagaki, Y. Utsuno, J. Vary, P. Maris, and H. Ueno, Nature Communications **13**, 2234 (2022).
[31] J.-P. Ebran, E. Khan, T. Nikšić, and D. Vretenar, Nature **487**, 341 (2012).
[32] J. Magill, J. Galy, and T. Žagar, in *Lasers and Nuclei: Applications of Ultrahigh Intensity Lasers in Nuclear Science* (Springer, 2006).
[33] J. Magill and J. Galy, *Radioactivity, radionuclides, radiation*, Vol. 259 (Springer, 2005).
[34] G. Gamow, Zeitschrift für Physik **51**, 204 (1928).
[35] C. Simenel, The European Physical Journal A **48**, 152 (2012).
[36] V. Y. Denisov and W. Nörenberg, The European Physical Journal A-Hadrons and Nuclei **15**, 375 (2002).
[37] K. Washiyama and D. Lacroix, Physical Review C **78**, 024610 (2008).
[38] X.-X. Sun and L. Guo, Physical Review C **107**, L011601 (2023).
[39] X.-X. Sun and L. Guo, Physical Review C **107**, 064609 (2023).
[40] C. Simenel, A. Umar, K. Godbey, M. Dasgupta, and D. Hinde, Physical Review C **95**, 031601 (2017).
[41] H. Rose and G. Jones, Nature **307**, 245 (1984).
[42] R. Kumar, Physical Review C **86**, 044612 (2012).
[43] R. Kumar and M. K. Sharma, Physical Review C **85**, 054612 (2012).
[44] Z. Ren, C. Xu, and Z. Wang, Physical Review C **70**, 034304 (2004).
[45] Y. Qian and Z. Ren, Journal of Physics G: Nuclear and Particle Physics **39**, 015103 (2011).
[46] D. Ni, Z. Ren, T. Dong, and C. Xu, Physical Review C **78**, 044310 (2008).
[47] G. Röpke, P. Schuck, Y. Funaki, H. Horiuchi, Z. Ren, A. Tohsaki, C. Xu, T. Yamada, and B. Zhou, Physical Review C **90**, 034304 (2014).
[48] S. Yang, R. Li, and C. Xu, Physical Review C **108**, L021303 (2023).
[49] C. Xu and Z. Ren, Nuclear Physics A **760**, 303 (2005).
[50] C. Xu and Z. Ren, Physical Review C **73**, 041301 (2006).
[51] C. Xu and Z. Ren, Physical Review C **74**, 014304 (2006).
[52] D. Ni and Z. Ren, Physical Review C **82**, 024311 (2010).
[53] L.-J. Qi, D.-M. Zhang, S. Luo, G.-Q. Zhang, P.-C. Chu, X.-J. Wu, and X.-H. Li, Physical Review C **108**, 014325 (2023).
[54] J. A. Maruhn, P.-G. Reinhard, P. Stevenson, and A. S. Umar, Computer Physics Communications **185**, 2195 (2014).
[55] B. Schuetrumpf, P.-G. Reinhard, P. Stevenson, A. S. Umar, and J. A. Maruhn, Computer Physics Communications **229**, 211 (2018).
[56] P. Stevenson, Y. Shi, E. Yüksel, A. Umar, *et al.*, Computer Physics Communications **301**, 109239 (2024).
[57] C. Simenel and A. Umar, Progress in Particle and Nuclear Physics **103**, 19 (2018).
[58] E. Chabanat, P. Bonche, P. Haensel, J. Meyer, and R. Schaeffer, Nuclear Physics A **635**, 231 (1998).
[59] P. Eckle, A. Pfeiffer, C. Cirelli, A. Staudte, R. Dorner, H. Muller, M. Buttiker, and U. Keller, science **322**, 1525 (2008).
[60] X. Wang, J. Tian, and J. Eberly, Physical Review Letters **110**, 073001 (2013).
[61] J. Schwinger, Physical Review **82**, 664 (1951).